# GEM-3: A Monostatic Broadband Electromagnetic Induction Sensor

I.J. Won, Dean A. Keiswetter, David R. Hanson
Elena Novikova and Thomas M. Hall

Geophex, Ltd.

## ABSTRACT

We have designed, fabricated, and field-tested a new, unique, monostatic, broadband, electromagnetic sensor for subsurface geophysical investigation. The sensing unit consists of a pair of concentric, circular coils that transmit a continuous, broadband, digitally-controlled, electromagnetic waveform. The two transmitter coils, with precisely computed dimensions and placement, create a zone of magnetic cavity (viz., an area with a vanishing primary magnetic flux) at the center of the two coils. A third receiving coil is placed within this magnetic cavity so that it senses only the weak, secondary field returned from the earth and buried targets.

This monostatic configuration has many advantages including (1) compact sensor head, (2) a large transmitter moment, (3) high spatial resolution, (4) no spatial distortion of an anomaly common to bistatic sensors, (5) circular symmetry that greatly simplifies mathematical description, and, therefore, (6) simplified forward and inverse modeling processes. Three prototype GEM-3 units have been built and tested at various environmental sites, including those containing unexploded ordnance and land mines.

## Introduction

Based on the data quality and quantity, portability, and non-intrusiveness, the electromagnetic induction (EMI) method is perhaps the most popular method for shallow geophysical exploration. During the past several years, Geophex has developed a new generation of airborne and man-portable EMI sensors. GEM-2, first debuted in early 1995, is a 9-lb hand-held, bistatic EMI sensor that can operate either in the frequency- or the time-domain mode. In the frequency-domain, GEM-2 is field-programmable to operate at simultaneous, multiple frequencies or in swept-frequency mode between 90 Hz and about 24 kHz. The GEM-2 operating principles and case histories are described in Won et al. (1996).

One of the major motives for GEM-3 was to increase lateral and spatial resolution. A bistatic sensor, because of the long path between the source and receiver, is inherently poor in spatial resolution particularly for small, shallow targets. Figure 1 shows GEM-3 in operation as of August, 1996. For this prototype, the electronic console including the data logger is very similar to that of GEM-2. Figure 2 shows the electronic block diagram of GEM-3.

## GEM-3 Operating Principle

The GEM-3 sensor contains a pair of concentric transmitter coils and a small receiver coil at the center. We call this concentric geometry a "monostatic" configuration because all coils are essentially co-located. The GEM-3 is a transmitter-bucked sensor, as will be discussed in a later section. All coils are molded into a single, light, circular disk in a fixed geometry, rendering a very portable package. The disk, along with a handle boom, is made of a Kevlar-skinned foam board. Attached to the other end of the boom is a removable electronic console (fig.1).

For a frequency-domain operation, the GEM-3 prompts for a set of desired transmitter frequencies. Built-in software converts these frequencies into a digital "bit-stream," which is used to construct the desired transmitter waveform for a particular survey. This bit-stream represents the instruction on how to control a set of digital switches (called H-bridge) connected across the transmitter coil, and generates a complex waveform that contains all frequencies specified by the operator. This method of constructing an arbitrary waveform from a digital bit-stream is known as the pulse-width modulation (PWM) technique.

The base period of the bit-stream for GEM-3 is set to 1/30th of a second for areas having a 60-Hz power supply, as does the U.S. The period is 1/25th of a second at 50-Hz areas, as in Europe and Japan. The GEM-3 H-bridge switches at a rate of 96 kHz and, therefore, the bit-stream contains 3,200 steps within the 1/30-second base period. Any integral number of the base period may be used for a consecutive transmission in order to enhance the signal-to-noise ratio (SNR). For detailed explanation of how the GEM-2 constructs a transmitter waveform and actual examples, refer to Won et al. (1996).

## Bistatic and Monostatic Sensors

The terms "bistatic" and "monostatic" may be new to some readers; hence, a brief discussion is appropriate. As a simple analogy, an underground miner who uses a headlamp operates a monostatic sensor because his light source and eyes are essentially co-located. A camera with a built-in flash

**Figure 1. GEM-3 in operation. The entire unit weighs about 9 lbs and has a data-logging capacity of about 50,000 points before downloading.**

would also be analogous. However, if the miner has his own lamp broken, and relies on a fellow miner's lamp some distance away, he then operates a bistatic sensor because the light source and his eyes are no longer co-located. The miner in this case will observe more shadows because the light impinges at oblique angles with respect to his line of sight. Other than the shadows, the situation does not systematically affect how far he can see.

The majority of geophysical sensors are bistatic. Common examples include seismic refraction and reflection arrays, all DC electrical arrays (Wenner, Schlumberger, etc.), certain ground-probing radars (GPR), and most active frequency-domain EMI sensors. All bistatic sensors measure some sort of integrated properties of the medium between the source and receiver. The exact path or volume of integration depends on the governing physics, source-receiver geometry, medium properties, and, in the case of waves, raypath and source frequency. The measured properties may be the travel time (seismic and GPR), potential differences (DC resistivity), or changes in the amplitude, phase, or decay rate in time (EMI).

Monostatic geophysical sensors, where the source and receiver are co-located, are relatively rare; examples may include marine acoustic profilers and depth sounders, certain GPRs, and some time-domain EMI sensors. Monostatic sensors have many advantages over bistatic sensors: they are compact, light, easy in logistics, and the operating principles are often mathematically simple to describe. The practical difficulty of monostatic sensors, however, is that the receiver must be able to sense a small return signal in the presence of the large source signal, or measure the signal only while the source is turned off or sufficiently attenuated.

### Source-Receiver Separation vs. Depth of Exploration

Because most geophysical sensors are bistatic, we often associate the separation between the source and receiver as the major operating variable in order to interpret the data. There is a pervasive misconception, however, that the separation between the source and receiver ultimately governs the depth of exploration. If that is indeed the case, a monostatic sensor should not be able to see any depth at all!

This notion may have been partly derived from the familiar DC resistivity method where the current path does extend deeper as the two source electrodes expand in distance. A finite source-receiver distance is also necessary for certain ray-tracing methods, requiring observation of a particular raypath that emerges only beyond a certain distance. Refraction seismology is a prime example. For most other geophysical methods, including the EMI method, there is no systematic connection between the source-receiver separation and the depth of exploration.

Let us expound on this misconception using the EMI method as the example, even though a similar explanation would apply to most active-source geophysical sensors. *The sole purpose of an EMI source is to induce a secondary current into the earth.* This role of the source is the same whether in the frequency-domain or the time-domain. For a given source, the current induced in the earth depends solely on where it is located. *In fact, the source does not recognize, or even care, whether there is a receiver nearby, or anywhere.* It is clear, therefore, that the existence of a receiver by no means affects the shape of induced current field in the earth (aside from the uncertainty principle of the quantum theory!).

In other words, the earth volume affected by the source (thus the current distribution as a function of depth, or the depth of exploration) has already been determined by the source, long before we place a single receiver anywhere. For an EMI source at a given spot, placed over an earth having a given conductivity structure, the only means of altering the induced current is changing the source frequency. The current distribution is governed by the well-known skin-depth effect: a low-frequency signal can travel far through a conductive earth and, thus, "sees" deep structures, while a high-frequency signal can travel only a short distance and, thus, "sees" only shallow structures (Won, 1980 and 1983). The travel distance depends also on the source strength, because the receiver must maintain an acceptable SNR threshold. This

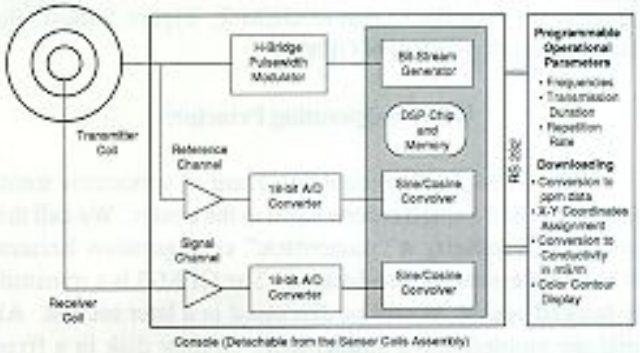


**Figure 2. GEM-3 electronic block diagram.**

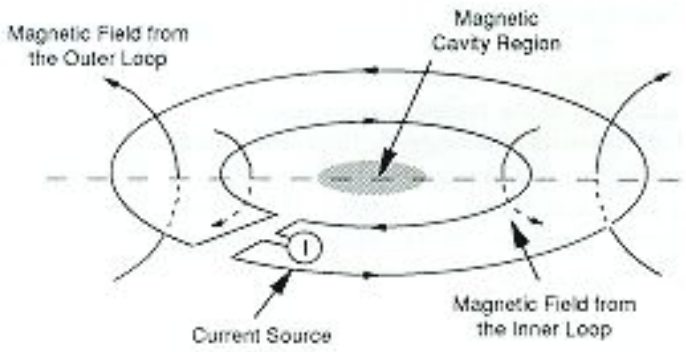


**Figure 3. Conceptual representation of creating a central magnetic cavity region using two concentric circular loops that are electrically connected in an opposing polarity.**

is the basis for the "frequency sounding" method. A critical requirement for a good frequency-sounding system is to insure a wide enough bandwidth to measure targets' spectral response.

Now, let us turn our attention to the receiver. The purpose of an EMI receiver is to measure the secondary electromagnetic field, usually by means of measuring a complex voltage (i.e., amplitude and phase) across a pickup coil. The measurement represents a weighted volume integral of the entire current distribution in the earth. The receiver location affects only the shape of the weighting function (commonly referred to as the kernel or Green's function) used for the integration of the induced current distribution.

When the receiver is close to the source, it is also generally close to the current induced in the earth and, therefore, the measured secondary field is strong. The opposite would be the case when the receiver is located far from the source. To determine the half-space conductivity, for instance, the measurement must be somehow normalized against the source-receiver separation. For a layered earth model, common to many EMI data interpretation techniques, the source-receiver separation, as well as the layer conductivities, appears as a part of the integral. Techniques that exploit this integral relation that involves the source-receiver separation are called the "geometrical sounding" methods. The word "sounding" in this case is somewhat misleading, however, because the source-receiver distance by no means affects the induced current pattern. In other words, a receiver located further away from the source does not make the source illuminate more deeply, or result in deeper "sounding" by the source field.

By now, it should be clear that the source-receiver separation has little to do with the depth of exploration. One may wonder then why all commercial EMI sensors are built in a bistatic geometry. The practical reason for this geometry is to avoid the strong primary field near the source, which decays rapidly at a rate of distance-cubed. The secondary field, resulting from the induced current in the earth, is very small and is difficult to measure in the presence of a large source field. Possible solutions for this problem includes (1) moving the receiver away from the source to avoid the strong field, or (2) increasing the dynamic range of the receiver electronic circuits. The former happens to be an easier solution at this time and, thus, is common to commercial bistatic EMI sensors.

There are additional remedies for this strong primary field problem. One solution is to measure the secondary field only when the source is turned off; this is the case for the time-domain EMI sensors that are often built in a monostatic geometry. The other solution is to make the source field "invisible" at the receiver location by "bucking out" the source field by connecting a small secondary receiver in an opposite polarity. This secondary receiver is called the "bucking" coil. The bucking design has been in use for several decades now, particularly for airborne EMI sensors for mining surveys, as well as in the existing GEM-2 (Won et al., 1996). *Once the source field can be bucked out, the receiver can be placed anywhere, and even can be co-located with the source.*

The GEM-2 is known as a receiver-bucked sensor because a small additional receiver coil bucks out the source field. On the other hand, the GEM-3 achieves the bucking by adding a second transmitter coil and, therefore, is considered a transmitter-bucked sensor.

### Monostatic Sensor and High Spatial Resolution

A bistatic sensor tends to stretch or distort an isolated anomaly along the line connecting the source and receiver. For instance, a spherical object may appear to be oval-shaped, stretched along the source-receiver line on a contour map. Because of this direction-dependent anomaly pattern, the same object may look different on a contoured map depending on the sensor orientation; this can be an annoying feature for interpretation. The stretching typically increases with the source-receiver separation.

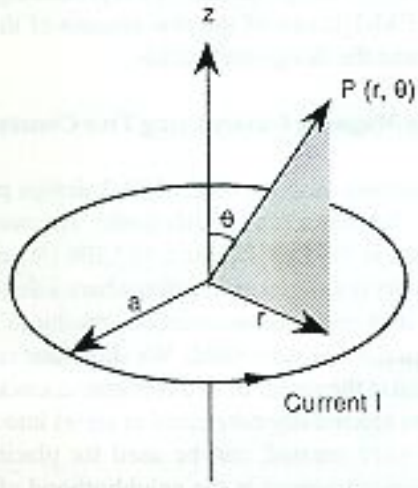


**Figure 4. Geometry for computing magnetic near-field for a single current-carrying circular loop.**

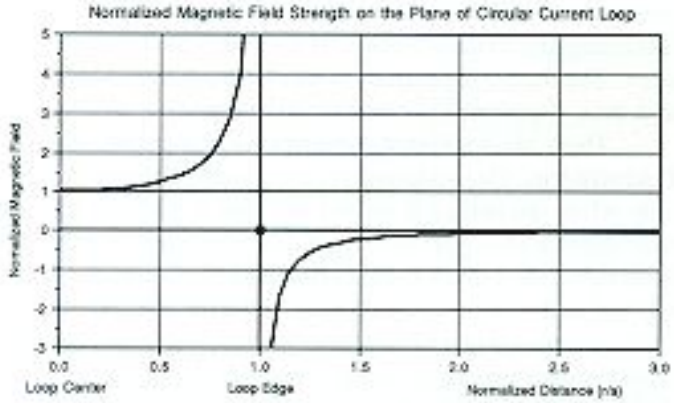


**Figure 5. Normalized magnetic field strength as a function of radial distance on the plane of a circular current loop. Actual magnetic field may be computed by multiplying to the normalized amplitude.**

A familiar textbook example is how a normal fault appears under a Wenner resistivity profile; the fault is stretched over the entire distance involving the four-electrode array. Point-measurement sensors (such as a gravimeter or a magnetometer for the potential field methods) as well as most monostatic sensors do not manifest such a sensor-dependent stretching, mainly because their sensing footprint is isotropic and has a circular symmetry.

An anomaly stretched or distorted by the source-receiver geometry degrades the spatial or lateral resolution in pinpointing isolated targets such as buried trenches, underground storage tanks, or land mines. Zero source-receiver separation, i.e., a monostatic sensor, eliminates stretching and, therefore, provides the highest spatial resolution. In reflection seismics, the shotpoint-geophone separation is artificially reduced to zero during the processing through the "normal move-out" operation.

A monostatic sensor is the most desirable geophysical sensor for achieving high spatial resolution. However, there are many practical design difficulties in producing such a sensor. The GEM-3 is one of the few sensors of this kind that have overcome the design difficulties.

### Design of a Magnetic Cavity Using Two Concentric Coils

This section describes the GEM-3 design principle involving two concentric transmitter coils. The concept is further described in the U.S. Patent 5,557,206 (Won, 1996). A magnetic cavity is defined as a region where a directional sensor, placed in a specified orientation, produces zero signal induced from the magnetic field. We show that such a cavity can be created at the center of two concentric, circular, current loops that are electrically connected in series into one circuit. The cavity, once created, can be used for placing a highly sensitive magnetic sensor in the neighborhood of a large active, dipolar magnetic field. The concept is schematically shown in fig. 3.

Near Magnetic Field of a Circular Current Loop

Since the magnetic cavity is to be created at the center of a current-carrying loop, we first analyze the near-field characteristics of the magnetic field generated by a single loop. Let us consider the magnetic field at an arbitrary point $P(r, \theta)$ off the axis of a circular loop as shown in fig. 4. The loop has a radius a and carries a current $I$. Owing to the obvious azimuthal symmetry, we can express the scalar magnetic potential function $V_m$ as

$$V_m(r,\theta) = A_0 P_0(\cos\theta) + A_1' P_1(\cos\theta) + \ldots + \frac{B_0}{r} + \frac{B_1}{r^2} P_1(\cos\theta) + \ldots \quad (1)$$

where $V_m$ satisfies Laplace equation $\nabla^2 V_m = 0$ and $P_n$ is the $n$-th order Legendre function. On the axis along $\theta = 0$, $V_m$ can be analytically shown to be

$$V_m(r = z;\ \theta = 0) = \frac{\mu_0 I}{2}\left(1 - \frac{z}{\sqrt{a^2 + z^2}}\right) \quad (2)$$

which is true for any value z along the axis. Magnetic permeability of free space $\mu_0$ has a value of $4\pi \cdot 10^{-7}$ henry/m. Eq. (2) may be expanded into a Taylor series in terms of either $(a/z)$ for $a<z$ or $(z/a)$ for $a>z$, depending on whether the point $P(r, \theta)$ is within or outside the loop. By comparing the coefficients of the power series with those of Eq. (1), we can derive the following two equations:

$$V_m(r,\theta) = \frac{\mu_0 I}{2}\left[1 - \left(\frac{r}{a}\right)P_1(\cos\theta) + \frac{1}{2}\left(\frac{r}{a}\right)^2 P_2(\cos\theta) + \left(\frac{r}{a}\right)^3 P_3(\cos\theta) + \ldots\right] \text{ for } r \le a \quad (3a)$$

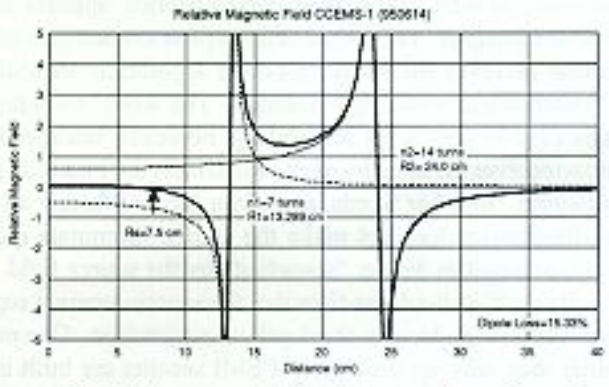


**Figure 6. Relative magnetic field strength as a function of radial distance for a three-coil system given R1 = 13.29 cm, n1 = 7, R2 = 24 cm, n2 = 14, and Rs = 7.5 cm. Total field (thick line) is the sum of the fields from the outer coil (thin line) and the inner coil (dotted line). Notice that the effect of the opposing inner coil is negligible to the far-field strength.**

and

$$V_m(r,\theta) = \frac{\mu_0 I}{2}\left[\frac{1}{2}\left(\frac{a}{r}\right)^2 P_1(\cos\theta) - \frac{3}{8}\left(\frac{a}{r}\right)^4 P_3(\cos\theta) + \ldots\right] \quad \text{for } r \geq a \qquad (3b)$$

It is easy to prove that at $r = a$, Eqs. (3a) and (3b) produce an identical value. Vector magnetic field $\mathbf{B}(r,\theta)$ can be derived from the potential function through

$$\boldsymbol{B}(r,\theta) = -\nabla V_m(r,\theta) \qquad (4)$$

for which $B_z$, the field perpendicular to the plane of the loop, may be computed by

$$B_z = -\cos\theta \frac{\partial V_m}{\partial r} + \frac{\sin\theta}{r}\frac{\partial V_m}{\partial \theta} \qquad (5)$$

Taking derivatives as required in Eq. (5) and letting $\theta$=90° (i.e., component perpendicular to the loop plane), we obtain the magnetic field as a function of radial distance $r$ on the plane of the loop:

$$B_z(r) = \frac{\mu_0 I}{2a}\left[1 + \left(\frac{1}{2}\right)^2 3\left(\frac{r}{a}\right)^2 + \left(\frac{1\cdot3}{2\cdot4}\right)^2 5\left(\frac{r}{a}\right)^4 + \left(\frac{1\cdot3\cdot5}{2\cdot4\cdot6}\right)^2 7\left(\frac{r}{a}\right)^6 + \ldots\right]$$

(6a) for $r \leq a$; inside the loop;

and

$$B_z(r) = -\frac{\mu_0 I}{2a}\left(\frac{a}{r}\right)^3\left[\frac{1}{2} + \left(\frac{1\cdot3}{2\cdot4}\right)^2 4\left(\frac{a}{r}\right)^2 + \left(\frac{1\cdot3\cdot5}{2\cdot4\cdot6}\right)^2 6\left(\frac{a}{r}\right)^4 + \ldots\right]$$

(6b) for $r \geq a$; outside the loop.

It is easy to show that as $r$ becomes much greater than $a$, the far-field approximation yields

$$B_z(r) = -\frac{\mu_0 I a^2}{4r^3} = -\frac{\mu_0 M}{4\pi r^3}$$

*where* M *(magnetic moment)* = $I\pi a^2$ *(7)*

which is the classical expression for a dipolar magnetic field. Figure 5, as an example, shows $B_z(r)$ computed from Eqs. (6a) and (6b), as a function of normalized distance ($r/a$) on the plane of a circular current loop. The amplitude is also normalized to $\mu_0 I/(2a)$ at $r$=0, the loop center. Notice that the magnetic field at the center of the loop is flat, having a vanishing gradient. Far-field strength, as the distance increases, essentially follows Eq. (7). Notice that the field at the center is strong yet spatially stable as indicated by its flatness. This spatial stability is the major asset that enables us to create a magnetic cavity by means of superimposing an opposite, yet also stable, magnetic field generated by a small concentric loop.

Creation of a Central Magnetic Cavity Using Two Opposing Current Loops

Figure 3 shows the basic concept of creating a magnetic cavity using two loops; a series circuit of two connected loops carrying the same current in opposing directions. Let us assume that the two loops have the following parameters:

$R_1$: radius of the inner loop,
$n_1$: number of turns of the inner loop,
$R_2$: radius of the outer loop, and
$n_2$: number of turns of the outer loop.

At an arbitrary distance of r from the center but inside the inner loop, the magnetic field due to the inner loop is then

$$B_z^1(r) = \frac{\mu_0 I n_1}{2R_1}\left[1 + \left(\frac{1}{2}\right)^2 3\left(\frac{r}{R_1}\right)^2 + \left(\frac{1\cdot3}{2\cdot4}\right)^2 5\left(\frac{r}{R_1}\right)^4 + \left(\frac{1\cdot3\cdot5}{2\cdot4\cdot6}\right)^2 7\left(\frac{r}{R_1}\right)^6 + \ldots\right] \quad \text{for } r < R_1 \qquad (8a)$$

and, similarly, the magnetic field due to the outer loop is

$$B_z^2(r) = \frac{\mu_0 I n_2}{2R_2}\left[1 + \left(\frac{1}{2}\right)^2 3\left(\frac{r}{R_2}\right)^2 + \left(\frac{1\cdot3}{2\cdot4}\right)^2 5\left(\frac{r}{R_2}\right)^4 + \left(\frac{1\cdot3\cdot5}{2\cdot4\cdot6}\right)^2 7\left(\frac{r}{R_2}\right)^6 + \ldots\right] \quad \text{for } r < R_2 \qquad (8b)$$

We are interested in deriving a mathematical relationship among the coil parameters so as to create a magnetic cavity at the center of the coil pair. Let us place a third, con-

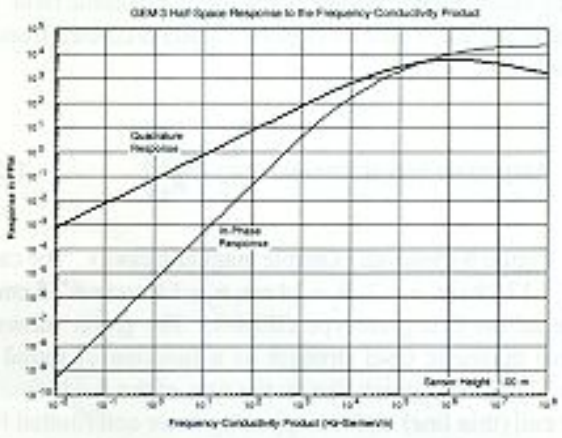


**Figure 7. GEM-3 interpretation chart for converting inphase and quadrature *ppm* data to earth conductivity.**

centric, circular loop having a radius $r$ that is less than $R_1$. This third loop is considered to be the receiver coil that is, in the absence of the primary field due to the magnetic cavity, designed to measure small variations in magnetic field induced from outside the coil system. The voltage output (*emf*) of the receiver coil would be proportional to the surface integral of the two opposing magnetic fields expressed by Eqs. (8a) and (8b):

$$emf = \int_0^r [B_2^2(r) - B_2^1(r)] \cdot 2\pi r \, d \, . \qquad (9)$$

For the magnetic cavity, we desire to have a vanishing emf. Therefore:

$$\int_0^r B_2^1(r) \, r \, dr = \int_0^r B_2^2(r) \, r \, d \, . \qquad (10)$$

Integrating Eqs. (8a) and (8b) and substituting them into Eq. (10), we obtain the following functional condition under which the output voltage of the receiver coil having a radius $r$ would be zero:

$$\frac{n_1}{R_1}\left[\frac{1}{2} + \left(\frac{1}{2}\right)^2\frac{3}{4}\left(\frac{r}{R_1}\right)^2 + \left(\frac{1\cdot3}{2\cdot4}\right)^2\frac{5}{6}\left(\frac{r}{R_1}\right)^4 + \left(\frac{1\cdot3\cdot5}{2\cdot4\cdot6}\right)^2\frac{7}{8}\left(\frac{r}{R_1}\right)^6 + \ldots\right]$$
$$= \frac{n_2}{R_2}\left[\frac{1}{2} + \left(\frac{1}{2}\right)^2\frac{3}{4}\left(\frac{r}{R_2}\right)^2 + \left(\frac{1\cdot3}{2\cdot4}\right)^2\frac{5}{6}\left(\frac{r}{R_2}\right)^4 + \left(\frac{1\cdot3\cdot5}{2\cdot4\cdot6}\right)^2\frac{7}{8}\left(\frac{r}{R_2}\right)^6 + \ldots\right]. \qquad (11)$$

Equation 11 provides the basic relation among the radii of the receiver coil and two concentric transmitter coils as well as the number of turns, which would result in zero sensor output voltage in free space.

While the outer coil, having a larger radius and more turns, is to be the principal transmitter of an active magnetic field, the inner coil due to its opposing magnetic polarity does slightly reduce the amplitude of the principal dipole field. The degree of the amplitude loss can be readily predicted from Eq. (7) such that:

$$\text{Amplitude loss at far field} = \frac{n_1}{n_2}\left(\frac{R_1}{R_2}\right) . \qquad (12)$$

Figure 6 shows an example magnetic cavity. The case is for $R_1 = 13.29$ cm, $n_1 = 7$, $R_2 = 24$ cm, $n_2 = 14$, and $r = 7.5$ cm, the values of the first prototype GEM-3. The graph shows the relative magnetic field strength as a function of radial distance. Total field (thick line) is the sum of the fields from the outer coil (thin line) and the opposing inner coil (dotted line).

We note that the magnetic field within the area encircled by the receiver coil is small and varies gently, starting positive at the center and slowly changing to negative toward the perimeter of the receiver coil. Areal integral of the magnetic field within the receiver coil, however, vanishes precisely according to Eq. (10) so as to produce zero voltage output by the receiver coil. Loss on the dipole strength of the outer coil for this case is 15.3% according to Eq. (12), a small amount as shown by the nearly unnoticeable changes in the far-field strength.

### GEM-3 Basic Measurement Unit

The inphase and quadrature data derived through the convolution (see fig. 2 for explanation) are converted into a part-per-million, or ppm, unit defined as:

$$ppm = 10^6 \cdot \frac{secondary\ magnetic\ field\ at\ receiver\ coil}{primary\ magnetic\ field\ at\ receiver\ coil} . \qquad (13)$$

These *ppm* values are the raw data logged by GEM-3. We note that the *ppm* unit defined by Eq. (13) is sensor-specific and has little physical meaning. The GEM-3 allows up to 50,000 data points before downloading to a PC through an RS-232 link. All parameters required for the *ppm* computation, such as the sensor output in free space (simulated by hanging GEM-3 from the top of a tall tree), and amplifier characteristics of the two receiving channels are stored in GEM-3 for real-time use.

In most shallow geophysical surveys, the *ppm* data generated by GEM-3, often plotted into a contour map at each frequency, are sufficient to locate buried objects without going through elaborate data processing or interpretation. One can also estimate the target depth from the data obtained at multiple frequencies.

### Conversion to Apparent Conductivity

The inphase and quadrature *ppm* data can be the raw input for any inversion software. Traditionally, however, EMI data is displayed in "apparent conductivity" by imagining that the earth below the sensor is represented by a homogeneous and isotropic halfspace. While the earth is heterogeneous with regard to geologic variations, it can be represented by an equivalent homogeneous halfspace that would result in the same observed data.

The total magnetic field measured at the center of, and perpendicular to, the GEM-3 disk can be written

$$H_z = \frac{M}{2\pi a^3} + \frac{M}{4\pi}\int_0^\infty \lambda^2 \frac{\lambda - \sqrt{\lambda^2 + k^2}}{\lambda + \sqrt{\lambda^2 + k^2}} e^{-2\lambda h} \, d\lambda \qquad (14)$$

where the first term represents the source field from the transmitter coil having a radius $a$ and a dipole moment $M$, and the

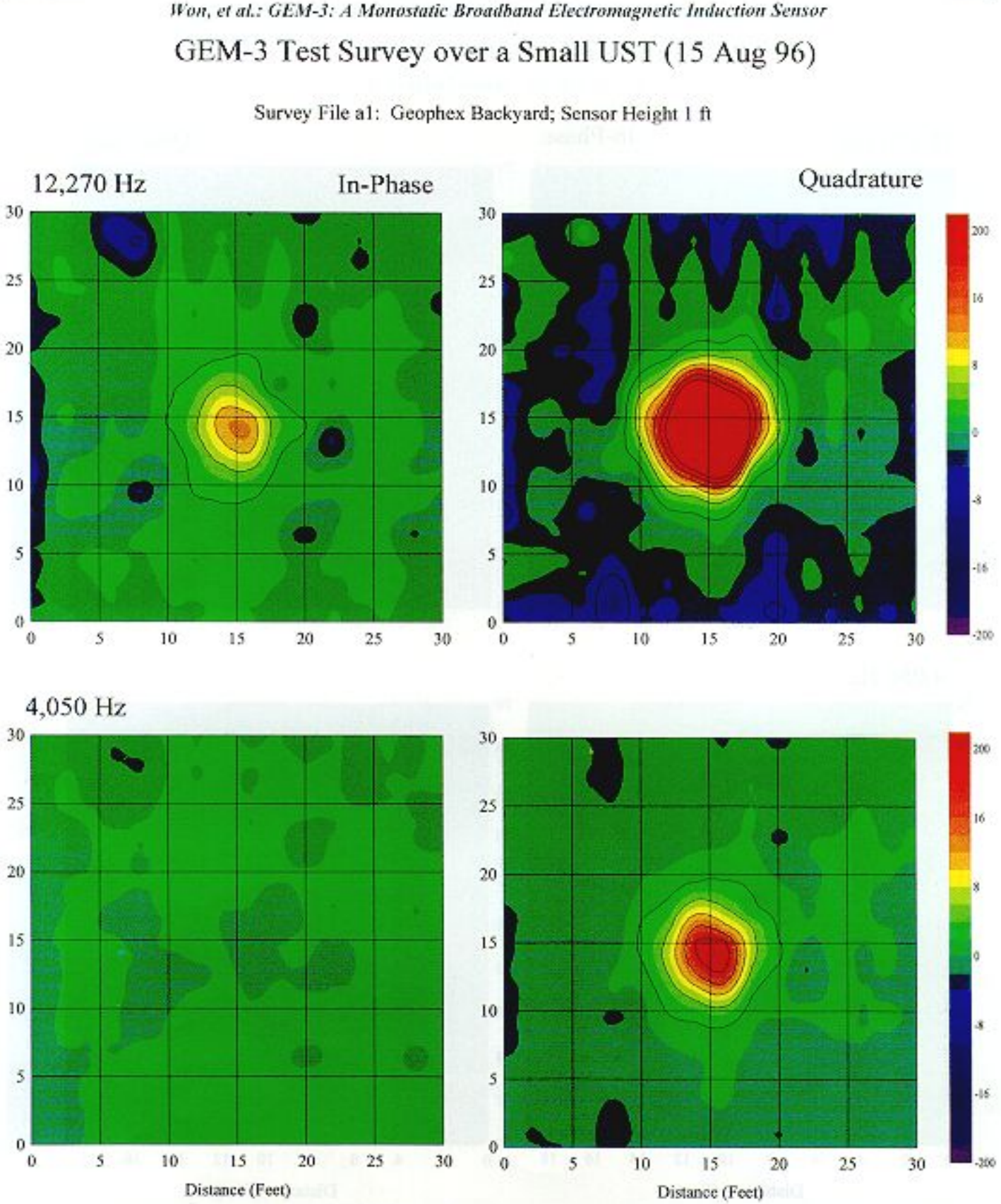


**Figure 8. GEM-3 response over a 225-gal underground storage tank buried at 6 feet in clay soil.**

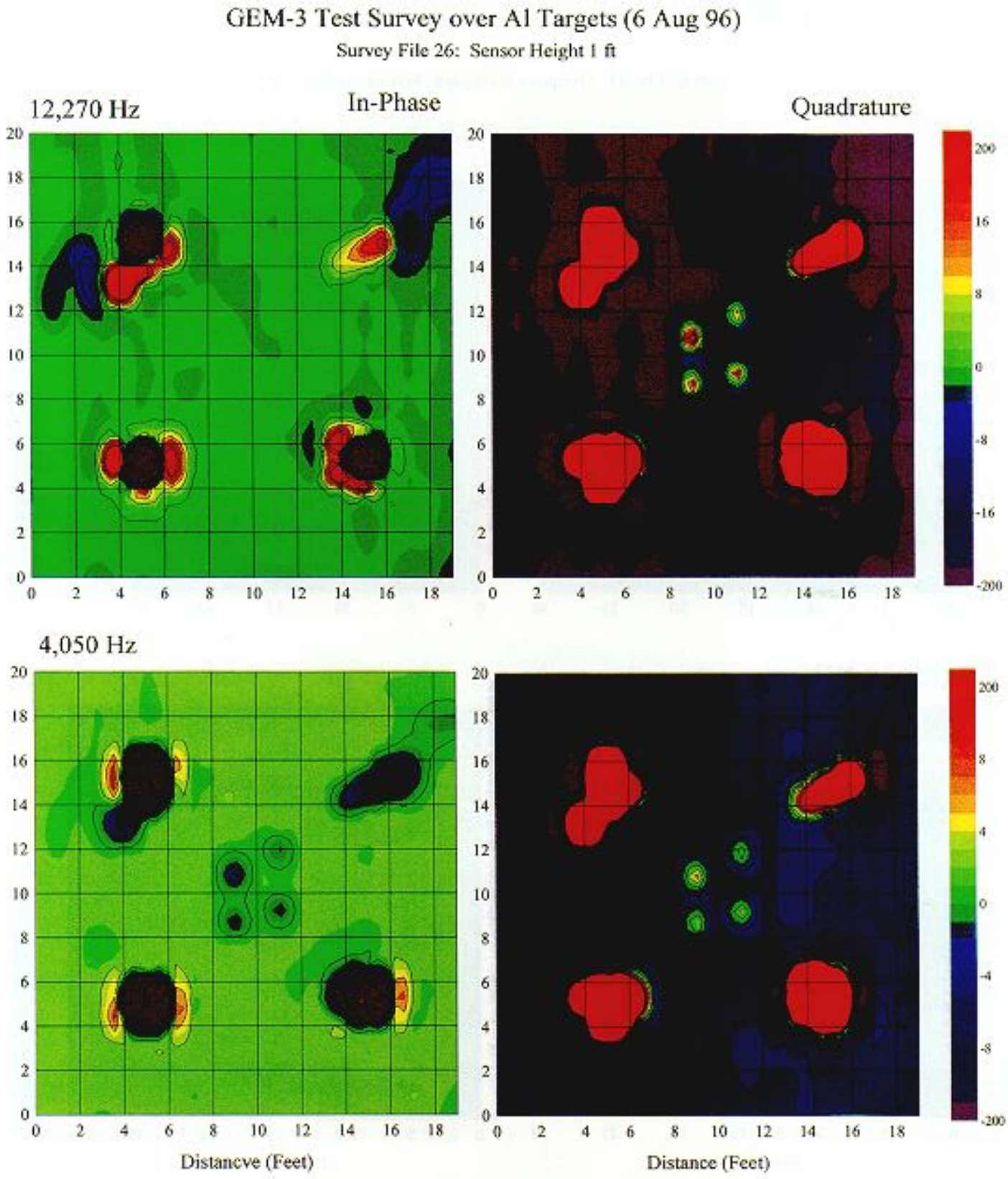


**Figure 9. GEM-3 response of aluminum disks on the surface. The four small targets are 2 inch diameter circles. Outer targets are 4 to 8 inches in diameter. All disks are 20-mil thick.**

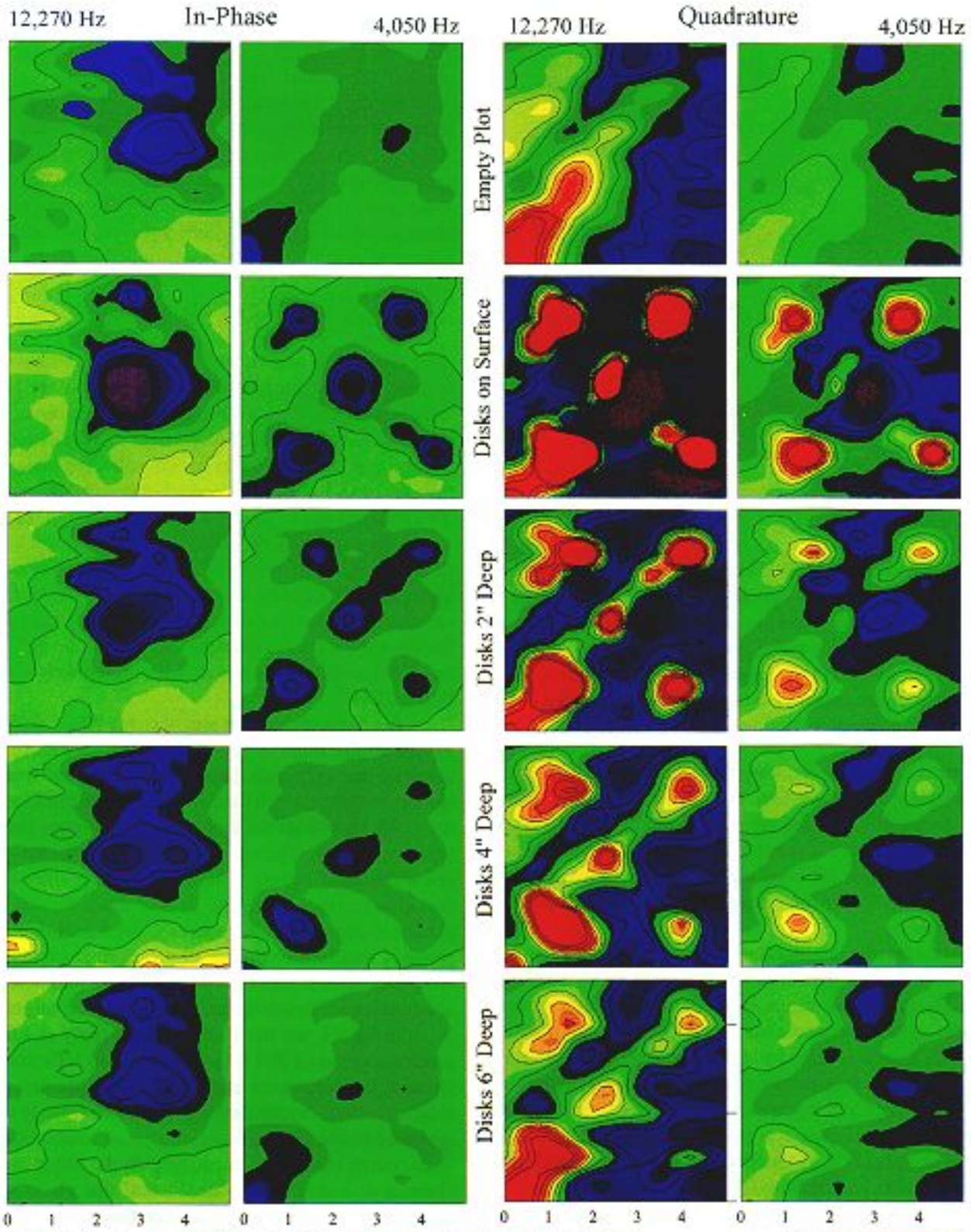


**Figure 10. GEM-3 response of a circular steel disk (at the center; 2.375 inch in diameter and 1/32-inch thick) and four circular aluminum disks (at four corners; 2 inch in diameter and 20-mil thick). The test area is 5 ft by 5 ft in size. The top row response of the test site without any targets. The next four rows show the targets buried at increasing depths.**

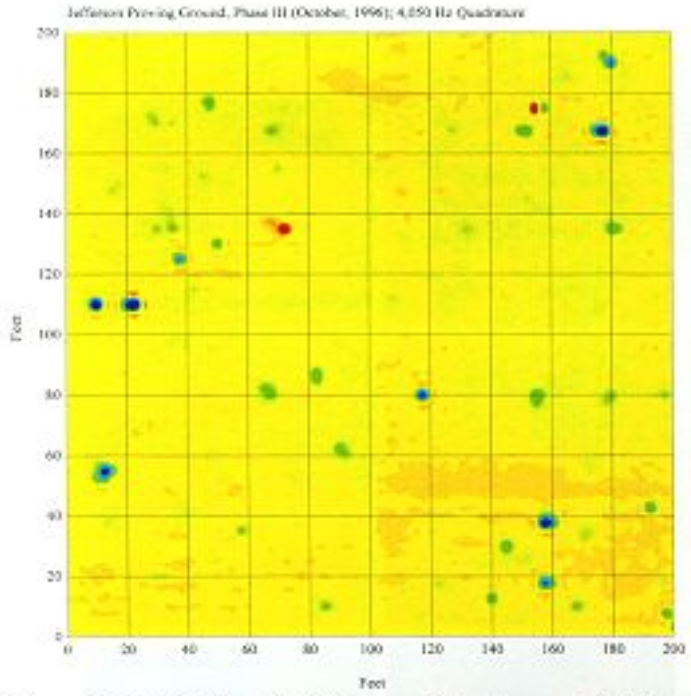


**Figure 11. GEM-3 data (4,050 Hz quadrature) over a 200 ft by 200 ft plot in the Jefferson Proving Ground, Indiana, where unexploded ordnance items are presumably buried. Notice the color variations (blue to red, corresponding to low to high) indicating phase reversals depending on metal types. Because of this phase rotation, a target may be detected only within certain frequency windows.**

second term is the field resulting from the induced current in the earth. Here, $k^2=i\omega\mu\sigma$ where $\omega$ is angular frequency, $\mu$ the magnetic susceptibility, and the $\sigma$ conductivity. The GEM-3 height above the earth is denoted by $h$ in Eq. (14). Unfortunately, we have not yet been able to derive a closed form integral of Eq. (14) and, thus, have relied on a numerical integration method.

Notice that the familiar Bessel function ubiquitous to all bistatic EMI sensors (Kozulin, 1963; Frischknecht, 1967) is gone in Eq. (14). The argument of Bessel functions in this case contains the source-receiver separation; for a monostatic sensor with a zero separation, $J_0(0)=1$ and $J_n(0)=0$ for all $n$ other than 1. This banishment of Bessel functions applies to both the halfspace and layered earth models. This is one of many mathematical beauties of a monostatic EMI sensor.

Dividing Eq. (14) by the first term on the right-hand side (the source field), and multiplying by one million, we can obtain the GEM-3 response over a halfspace in a *ppm* unit as follows:

$$ppm = 10^6 \cdot \frac{a^3}{2} \int_0^\infty \lambda^2 \frac{\lambda - \sqrt{\lambda^2 + k^2}}{\lambda + \sqrt{\lambda^2 + k^2}} e^{-2\lambda h} d\lambda. \quad (15)$$

We notice from Eq. (15) that conductivity and frequency appear as a single product in $k^2$. For multifrequency data, therefore, Eq. (15) provides the relationship between the *ppm* unit and the conductivity-frequency product.

Figure 7 shows the computed inphase and quadrature responses over halfspace for the GEM-3 horizontal coils. We assumed, for this example, a sensor height of 1 meter, the typical waist level for a surveyor. In essence, the observed ppm value (y-axis) determines the conductivity-frequency product (x-axis), which is then divided by the known transmitter frequency to obtain the halfspace conductivity.

## GEM-3 Field Data Examples

Since it debuted in mid-1996, the GEM-3 has been used at many environmental sites. In this section, we present selected examples. Figure 8 shows GEM-3 inphase and quadrature responses at two frequencies over a 225-gal. underground storage tank buried at 6 feet in clay soil. The tank, buried on the side, has a 3-ft diameter and a 5-ft length. The amplitude is not calibrated in this plot and is relative only in scale.

The capability of GEM-3 in detecting small targets is shown in fig. 9. In an area of 20 ft by 20 ft, we placed four 2-inch diameter, circular aluminum disks on the surface in the central area. Outer targets are also aluminum disks on surface having 4 to 8 inches in diameter. All aluminum disks were cut from 20-mil-thick sheet metal. All targets are clearly detected by the GEM-3.

In a much smaller test area of only 5 ft by 5 ft (fig. 10), we placed similar small targets: a circular steel disk (2.375-inch diameter and 1/32-inch thick) at the center and four circular aluminum disks (2-inch diameter and 20-mil thick) at four corners. We show both the inphase and quadrature responses at two frequencies. The top row shows the response of the test site without any targets. The next four rows show the targets buried at increasing depths. It is obvious that the anomaly pattern is dependent on frequency, the burial depth, and inphase or quadrature. Figure 10 demonstrates that the broadband data in both inphase and quadrature manifest different information for detecting and interpreting the targets.

In fig. 11, we show GEM-3 data (only at 4,050 Hz in quadrature) over a 200 ft by 200 ft plot in Jefferson Proving Ground, Indiana, where unexploded ordnance items presumably are buried. Notice the color variations (blue to red, corresponding to low to high) indicating phase rotations, which we found occur commonly depending on the target metal types (ferrous or non-ferrous). Because of this phase rotation, a target may be detected only within certain frequency windows, further supporting the need for multifrequency measurements.

Finally, fig. 12 shows the GEM-3 response at 12,270 Hz at Turkey Creek Test Site in Fort Carson, Colorado. The site includes five "registration targets" denoted by oval-shaped areas that contain buried objects to simulate unexploded ordnance. Each registration area contains an 8-inch aluminum square sheet (top) and a 16-lb steel shotput (bottom). We

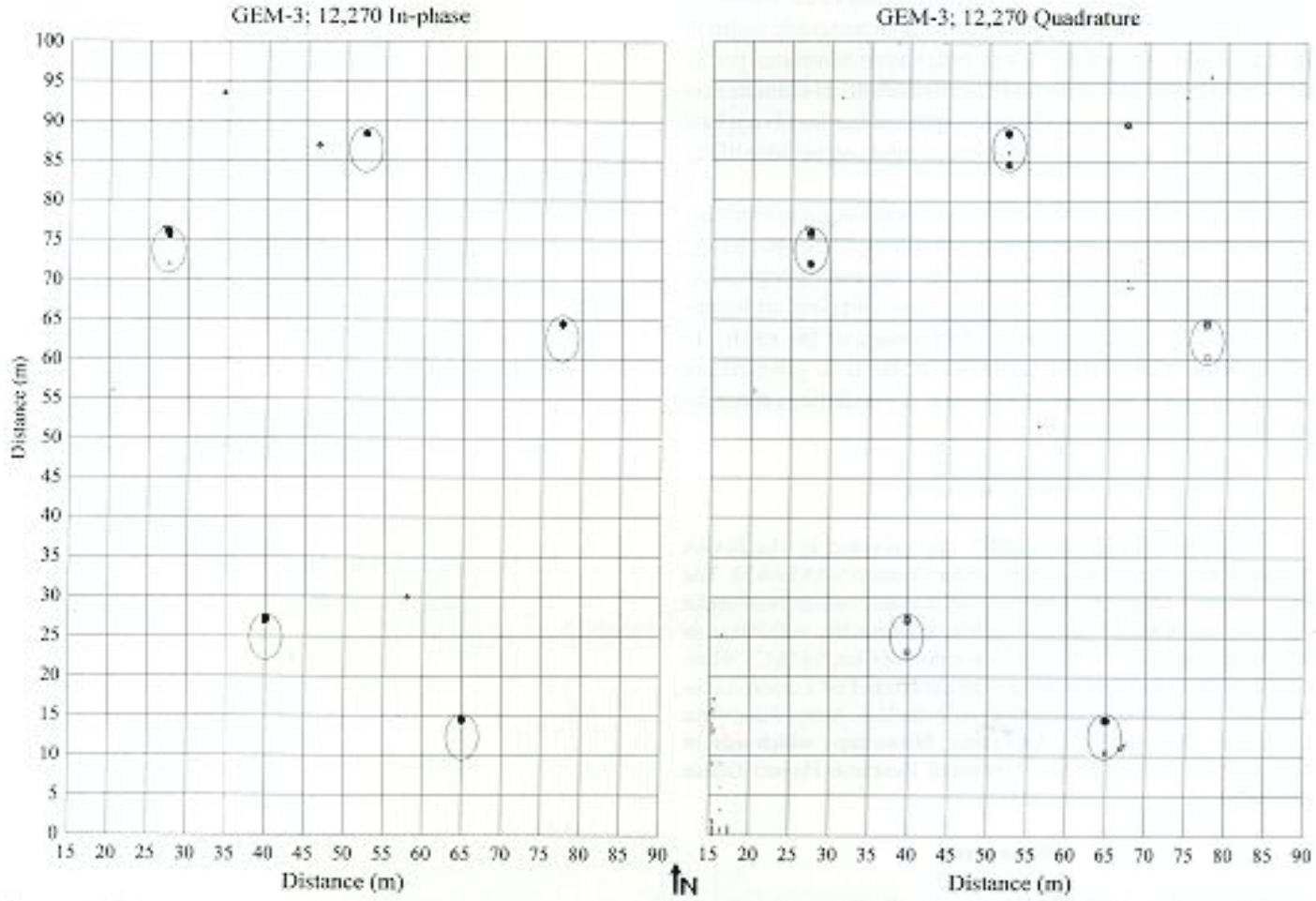


**Figure 12. GEM-3 response at 12,270 Hz quadrature at Turkey Creek Test Site in Fort Carson, Colorado. The site includes "registration targets" buried in five oval-shaped areas. Each registration area contains an 8-inch aluminum square (top) and a 16-lb steel shotput (bottom). Black dots in each oval are, in fact, made of many closely-spaced contours centered over the buried targets. We noted that the aluminum target is seen over a broadband while the shotput is not seen at certain frequency particularly in the inphase component.**

noted that the aluminum target is seen over a broadband while the shotput is not seen at certain frequencies, particularly for the inphase component.

## Conclusions

GEM-3 is a new, unique, monostatic, broadband, electromagnetic sensor for subsurface geophysical investigation. The GEM-3 is able to detect small targets such as buried ordnance and land mines with highest spatial resolution. The sensor is based on a well-founded physical principle of creating a precise magnetic cavity using two concentric transmitter coils. A receiver coil is placed within this magnetic cavity so that it can sense the weak, secondary field returned from the earth and buried targets.

This monostatic configuration has many advantages including compact sensor head, a large transmitter moment, high spatial resolution, no spatial distortion of an anomaly (as is common with bistatic sensors), circular symmetry that greatly simplifies mathematical description, and, therefore, simplified forward and inverse modeling processes. Three prototype GEM-3 units that have been built and tested at various environmental sites, including those containing unexploded ordnance and land mines, proved the advantages of the design concept.

The remaining hardware challenge for the further development of GEM-3 is increasing its operating bandwidth from the present 24 kHz to several hundred kilohertz. Once we can cover a few decades in frequency band employing an active EMI source, we should be able to measure a continuous spectral response of a given buried object. For GEM-3 (as well as for GEM-2), this can be achieved by either (1) sweeping through the entire band width one frequency at a time (Won, 1983), or (2) employing a fast Fourier transform technique during the data acquisition using a broadband source such as pseudo-random sequence pulses. Such a concept may be

called "EMI spectroscopy," or EMIS, that may cover from ELF to RF spectral bands. Like any other spectroscopic technology, the EMIS, once fully developed, has an enormous potential for target identification and discrimination, an ultimate sensor requirement for many detection applications involving land mines, airport security, and numerous other object identification needs.

The challenge on the software front is equally exciting. At this time, we have no means of examining a large amount of data in a broad band, particularly for an areal geophysical survey. A parallel effort is given to the inversion of broadband data to produce the subsurface image of the earth. In cooperation with several scientists in the U.S. government and universities, we hope to advance this ambitious theoretical front in the near future.

## Acknowledgments

Primary funding for GEM-3 was provided by the NASA Stennis Space Center, Mississippi, under Contract NAS13-670. The data from the Jefferson Probing Ground, Indiana, was obtained under a contract with PRC Environmental Management, Inc. which was, in turn, funded by the U.S. Army Environmental Center (AEC), Aberdeen Probing Ground, Maryland. The data from Fort Carson, Colorado, was obtained under a contract with the U.S. Army Waterways Experiment Station (WES), Vicksburg, Mississippi, which was, in turn, funded by the Defense Advanced Research Project Office (DARPA).

## References

Frischknecht, F.C., 1967, Field about an oscillating magnetic dipole over a two-layer earth and application to ground and airborne electromagnetic surveys, Quart. Colorado School of Mines, **62**, no. 1, pp. 1-370.

Kozulin, Y.N., 1963, A reflection method for computing the electromagnetic field above horizontal lamellar structures, Izvestiya, Academy of Sciences, USSR, Geophysics Series (English Edition), no. 2, pp. 267-273.

I.J. Won, 1980, A wideband electromagnetic exploration method - Some theoretical and experimental results, Geophysics, v. **45**, pp. 928-940.

I.J. Won, 1983, A sweep-frequency electromagnetic exploration method, Chapter 2, in Development of Geophysical Exploration Methods-4, Editor: A. A. Fitch, Elsevier Applied Science Publishers, Ltd., London, pp. 39-64.

I.J. Won, 1996, Apparatus and method for detecting a weak induced magnetic field by means of two concentric transmitter loops, U.S. Patent 5,557,206.

I.J. Won, Keiswetter, D.A., Fields, G.R.A., and Sutton, L.C., 1996, GEM-2: A new multifrequency electromagnetic sensor, J. Environmental and Engineering Geophysics, **1**, no. 2, pp. 129 - 138.